Acc. Sc. Torino
Atti Sc. Fis. 143 (2009)

On the Magnetization of Disk-Jet Systems

Nota di ATTILIO FERRARI[*], PETROS TZEFERACOS[**], ANDREA MIGNONE[***] e CLAUDIO ZANNI[***] presentata dal Socio corrispondente ATTILIO FERRARI nell'adunanza del 22 aprile 2009

Abstract. *In the framework of the study of jet acceleration from accretion disks in active galactic nuclei we discuss by non-relativistic 2.5 dimension numerical simulations how the strength of magnetic fields determine the characteristics of solutions in models where both the collimated outflow and the accretion disk are treated consistently. The main results are: (1) magnetic fields around and below equipartition with plasma pressure yield steady super-fast-magnetosonic collimated jet solutions; (2) for even lower magnetization solutions are unsteady, with field lines that behave kinematically; (3) magnetic fields above equipartition lead to unsteady sub-Alfvénic winds; (4) the configuration originally proposed by Blandford & Payne to interpret supersonic jets is viable for the range of parameters indicated.*

Keywords: Accretion discs, Jets and outflows, MHD, Methods: Numerical.

Riassunto. *Nell'ambito dello studio dell'accelerazione di getti supersonici da dischi di accrescimento in nuclei galattici attivi discutiamo sulla base di simulazioni numeriche a 2.5 dimensioni, non-relativistiche, gli effetti dell'intensità del campo magnetico nel determinare le caratteristiche delle soluzioni di modelli nei quali il flusso collimato di materia (getto) e il disco di accrescimento vengono trattati in modo consistente. I risultati di maggior importanza sono: (1) per campi magnetici vicino e sotto l'equipartizione con la pressione termica del plasma permettono la formazione di getti stabili con velocità superiori alla magnetosonica veloce; (2) per valori di magnetizzazione inferiori le soluzioni diventano intermittenti e le linee del campo magnetico si comportano in modo cinematico; (3) per campi magnetici sopra l'equipartizione si ottengono venti sub-Alfvénici; (4) la configurazione originariamente proposta da Blandford & Payne è valida per i parametri qui studiati.*

Parole chiave: Dischi di Accrescimento, Getti e Flussi, MHD, Metodi Numerici.

[*] Dipartimento di Fisica Generale, Università degli Studi di Torino, Via Giuria 1, 10125 Torino, Italy, e Department of Astronomy and Astrophysics, University of Chicago, USA.
[**] Dipartimento di Fisica Generale, Università degli Studi di Torino, Via Giuria 1, 10125 Torino, Italy.
[***] Dipartimento di Fisica Generale, Università degli Studi di Torino, Via Giuria 1, 10125 Torino, Italy, e INAF - Osservatorio Astronomico di Torino, Via Osservatorio 20, 10025 Pino Torinese, Italy.

1. Introduction

In pioneering works Lovelace (1976) and Blandford (1976) showed that a force-free poloidal field anchored in a Keplerian disk can extract energy and angular momentum from the accretion process and produce a collimated Poynting flux jet. This approach was later developed by Blandford & Payne (1982), who showed how a Poynting jet can transfer energy and momentum to outflowing matter via a magneto-centrifugal mechanism capable of reaching super-Alfvénic speeds. In these studies the disk was treated as a fixed boundary and no self-consistent treatment of the inflow/outflow dynamics was attempted.

In recent works Ferreira & Pelletier (1995), Ferreira (1997) and Casse & Ferreira (2000a,b) managed to link analytic "cold" and "warm" steady state outflow solutions with thin accretion disks. They conclude that super-Alfvénic outflows can be obtained with plasma β values around unity, for a limited range of Prandtl numbers and larger toroidal diffusivity.

The complexity of MHD equations, a time dependent non linear set of equations, leaves little hope for analytical studies to successfully follow the evolution of such a system: numerical simulations have been adopted to tackle the full problem. The first attempts referred to the entire disk-jet system, but for very short timescales (Uchida & Shibata, 1985; Kato et al., 2002). Casse & Keppens (2002) followed the evolution of an accretion-ejection system for longer timescales but without using an energy equation replaced by a simple polytropic equation of state; recently they updated their work including non-adiabatic effects (Casse & Keppens, 2004).

In a previous paper (Zanni et al., 2007) we have addressed the problem of the inflow/outflow dynamics on the basis of high-resolution compressible MHD numerical simulations, discussing the importance of resistive effects on defining stationary solutions. Here we concentrate on the strength of the initial magnetic field with respect to the possibility of reaching a stationary final state. Simulations have been performed in a 2.5D resistive framework, utilizing the numerical code PLUTO[1].

2. Setup

2.1. MHD equations

To model the accretion ejection system we solve numerically the equations of resistive magnetohydrodynamics:

$$\frac{\partial \rho}{\partial t} + \nabla \cdot (\rho \mathbf{u}) = 0, \tag{1}$$

[1] http://plutocode.to.astro.it, (Mignone et al., 2007)

$$\frac{\partial(\rho\mathbf{u})}{\partial t} + \nabla\cdot\left[\rho\mathbf{u}\mathbf{u} + \left(P + \frac{\mathbf{B}\cdot\mathbf{B}}{2}\right)\mathbf{I} - \mathbf{B}\mathbf{B}\right] + \rho\nabla\Phi_g = 0, \tag{2}$$

$$\frac{\partial\mathbf{B}}{\partial t} + \nabla\times\mathbf{E} = 0, \tag{3}$$

$$\frac{\partial e}{\partial t} + \nabla\cdot\left[\left(e + P + \frac{\mathbf{B}\cdot\mathbf{B}}{2}\right)\mathbf{u} - (\mathbf{u}\cdot\mathbf{B})\mathbf{B} + (\bar{\bar{\eta}}:\mathbf{J})\times\mathbf{B}\right] = -\Lambda_{cool}, \tag{4}$$

The primitive variables are density ρ, velocity $\mathbf{u}$, magnetic field $\mathbf{B}$ and thermal pressure p. The gravitational potential created by the central object of mass M is given in cylindrical coordinates by $\Phi_g = -GM/\sqrt{r^2+z^2}$. The electric field is obtained by Ohm's law, $\mathbf{E} = -\mathbf{u}\times\mathbf{B} + \bar{\bar{\eta}}:\mathbf{J}$ and the current $J = \nabla\times\mathbf{B}$ by Ampere's law. We assume for the magnetic resistivity a diagonal tensor η_{ij} with non-zero components $\eta_{\phi\phi} = \eta_m$ and $\eta_{rr} = \eta_{zz} = \eta'_m$. The symbol e denotes the total energy density:

$$e = \frac{P}{\gamma-1} + \frac{\rho\mathbf{u}\cdot\mathbf{u}}{2} + \frac{\mathbf{B}\cdot\mathbf{B}}{2} + \rho\Phi_g. \tag{5}$$

The term Λ_{cool} is a cooling function which in our study will be assumed proportional to the Ohmic heating term $\Lambda_{ohm} = f(\bar{\bar{\eta}}:\mathbf{J})\cdot\mathbf{J}$. We close the system with an ideal gas equation of state, with specific heat ratio $\gamma = 5/3$.

2.2. Model description

To model the accretion-ejection system we solve numerically the equations of resistive magnetohydrodynamics, neglecting all transport coefficients but for magnetic resistivity η_m. The latter is parametrized following the Shakura & Sunyaev (1973) paradigm,

$$\eta_m = \alpha V_A H \exp(-2z^2/H^2). \tag{6}$$

V_A denotes the Alfvén speed and H the thermal height scale, both calculated at the equator. The tensor representation of η_m allows for anisotropy in the magnetic diffusion and we specify the toroidal diffusion to be three times stronger than the poloidal. Even though we solve the energy equation, we assume that heating by Ohmic dissipation is fully radiated away. This is done to avoid a rise in the disk's entropy, being thus closer to the "cold" analytic solutions of Ferreira (1997).

The magnetic field strength, with respect to thermal pressure, is defined by the magnetization parameter $\mu = B^2/P$. We study four different cases of magnetization, below and above the limits set in the previously mentioned studies. From weak to strong field configurations, cases 1 to 4 correspond to values of

μ equal to 0.2, 0.6, 2.0 and 6.0 respectively. The initial inclination of the magnetic field lines is not varied here, but is set to a value, the same for all cases, that ensures an almost force-free initial field.

The initial configuration adopted considers a thin disk rotating at slightly sub-Keplerian speed with an embedded magnetic field with purely poloidal field lines exiting at some angle from the disk's surface. The field is initialized through its flux function to ensure solenoidality. The profiles of all other primitive variables are derived starting from an equatorial radial self-similarity assumption (Blandford & Payne, 1982) and imposing a force equilibrium in both radial and vertical directions. In pressure equilibrium with the disk's surface, we overimpose a static hot corona with radial stratification.

Our domain is a rectangular region spanning radially from 0 to $40r_0$ and vertically from 0 to $120r_0$. The temporal integration reaches ~ 63 revolutions of the disk's inner radius. Uniform resolution of $[512 \times 1536]$ is used throughout the domain.

Axisymmetry is assumed with respect to the rotation axis, and equatorial symmetry at the disk's midplane. At the upper and right boundaries special care has been used to maintain the magnetic field's solenoidality and to avoid artificial collimation. Since the origin is inside the computational domain, an appropriate internal boundary $[1.0r_{in} \times 0.5r_{in}]$ is imposed to cope with the singularity of the gravitational potential and the radial self-similar model there. No artificial outflow is allowed to escape that zone.

3. Results & Discussion

3.1. The effects of magnetization

The outflow driven from the disk displays a strong dependence on the choice of μ. In Fig. 1 we show the final form of the density distribution logarithm together with sample poloidal magnetic lines anchored at foot points on the disk equator.

For cases 1 and 2 with magnetic field below equipartition a light outflow is formed from the internal region of the disk progressively collimated by the magnetic field; the outer part of the disk generates a dense and slow disk wind, more prominent for low magnetization. Between the two, there is a difference in the time scale of collimation. For case 1 the magnetic field in the outer parts of the domain remains intermittently collimated. For magnetization closer to equipartition (case 2), the field lines relax to an open-field configuration. The disk geometry does not change substantially during the evolution.

For magnetization above equipartition (cases 3 and 4) the field topology becomes almost perpendicular to the disk. This confirms analytical studies (Fig. 2 in Ferreira, 1997) in which the increase of magnetization leads to a decrease of the field's curvature. The reason behind this is twofold. First of all, inside the disk, the magnetic resistivity is larger while the accretion speed

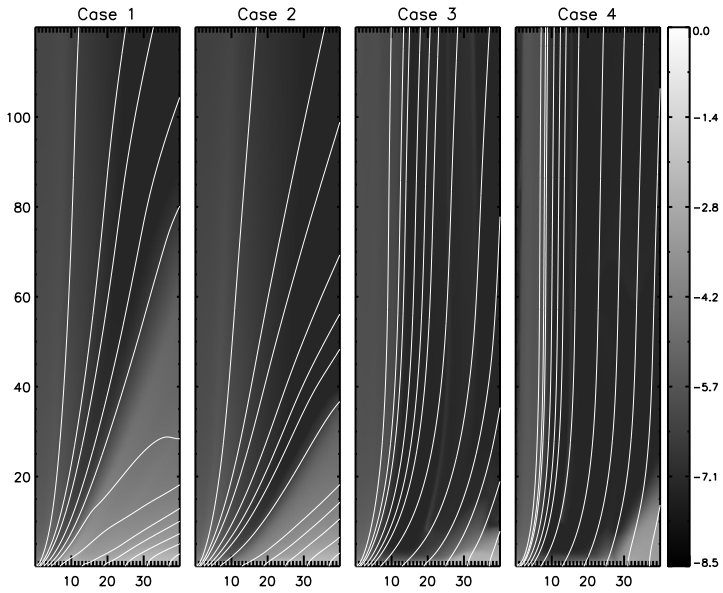

Figure 1: Logarithmic density and poloidal magnetic field for cases 1 to 4, after ~ 63 rotations ($t = 400$). The foot point of each field line is set to a same specific radius for all cases, in order to monitor the impact of magnetization in the collimation process.

decreases (Table 1.1) due to a weaker magnetic torque. This produces a relaxation that straightens the field lines near the base of the outflow, since the magnetic Reynolds number decreases and bending is not sustained. Secondly, in the upper part of the domain some degree of collimation is produced by magnetic tension. These factors lead to straight field lines and the initial vertical pinch of the radial field is reduced: the thermal pressure gradient is able to produce a denser outflow. Such a configuration does not favour the magneto-centrifugal mechanism due to the small inclination of the field lines added to a strongly sub-Keplerian rotation. The observed flattening of the accretion disk, on the other hand, is attributed to a pinch by the toroidal magnetic field (due to the initial azimuthal differential rotation) and the larger ejection rates. The absence of the extended outer wind is attributed to the small field inclination and deficient thermal push.

In Fig. 2 we plot the isocontours of the poloidal current for cases 1 to 4 at time $t = 30$. For values of μ below equipartition the current circuits follow the topology described in Ferreira (1997), whereas for cases 3 and 4 the result is somewhat unstable. The current flows anti-clockwise and the poloidal component of the Lorentz force is perpendicular to the isocontours and pointing outwards. This yields collimation of the magnetic surfaces in the inner part of the ouflow whereas the outer part de-collimates. As the current flows radially inside the disk towards the right boundary, the Lorentz force pinches the disk.

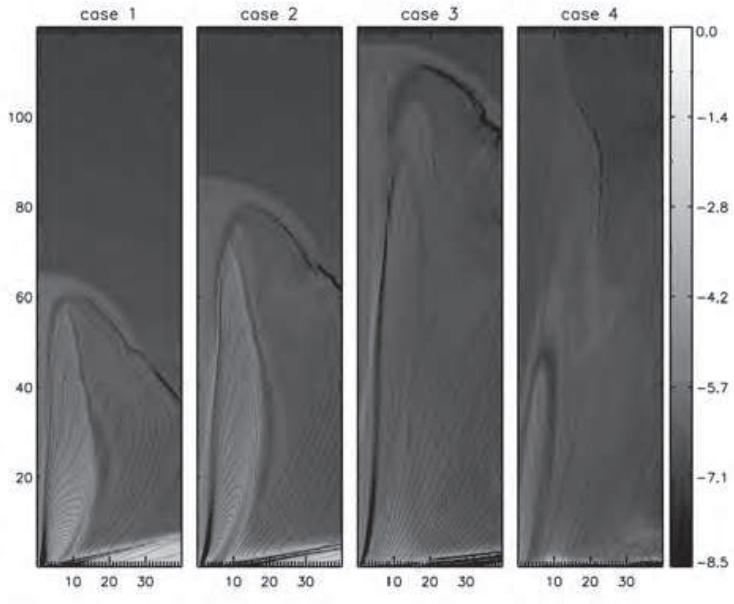

Figure 2: Four snapshots of the poloidal current distribution for the four cases studied, at time equal 30. For values of μ below equipartition the analytically expected butterfly topology is achieved, whereas for the magnetically dominated cases the outcome is unstable. The initial expansion is faster.

The efficiency of the magneto-centrifugal acceleration can be examined by the ability of the solutions to cross the critical surfaces, i.e. the isosurfaces where the poloidal velocity component becomes equal to one of the three MHD wave speeds: only solutions crossing these critical points produce steady outflows. In Fig. 3 we display the ratio of the poloidal over the fast magnetosonic velocity. The solid line is the Alfvénic surface, while vectors depict the poloidal flow lines.

The flow crosses the Alfvénic and fast-magnetosonic surfaces only for magnetization values below equipartition (i.e. cases 1 and 2). In cases 3 and 4 we can see that the outflow fails to become super-Alfvénic: Both the magnetic surface inclination (unavoidably violating the BP criterion and not promoting the conversion of magnetic to kinetic energy) and the slower rotation do not favour the magneto-centrifugal mechanism. Case 3 remains sub-Alfvénic while case 4 is mostly sub-slow.

3.2. Ejection efficiency and accretion properties - Reaching a steady state configuration

To examine the impact of the magnetic field strength on the rates of accretion and ejection, we introduce a control volume where these rates are calculated. This is delimited by the surfaces S_i and S_e perpendicular to the equator of

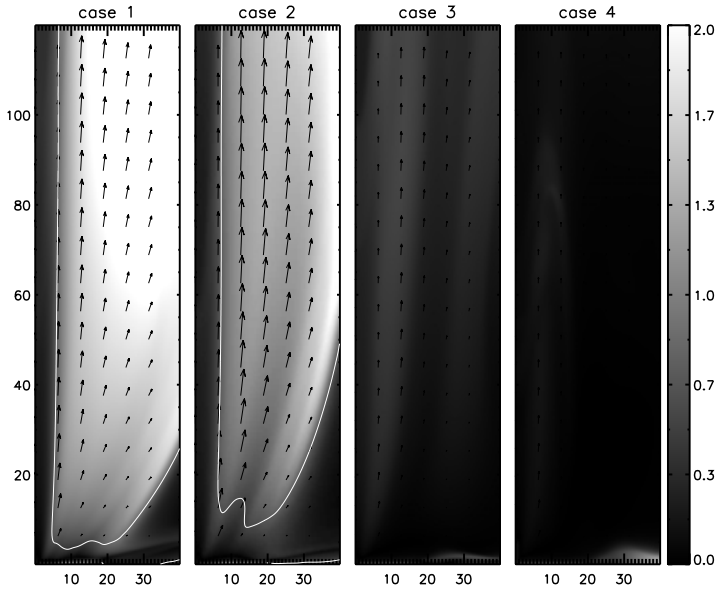

Figure 3: The effect of magnetization on the ability of the outflow to cross the critical surfaces. The figure displays snapshots at $t = 200$ of the poloidal velocity over the fast magnetosonic. The solid line indicates the Alfvénic surface and the poloidal velocity vectors are over-imposed.

the disk at $r_i = 1$ and $r_e = 10$ and height $2H(r_i)$ and $2H(r_e)$ respectively. The inclined surface on top of the disk, through which we calculate the ejection rates, will be denoted as S_d.

The mass flux entering the control volume from the S_e surface is given by the following integral:

$$\dot{M}_{acc} = -2\pi r \int_{-2H}^{2H} \rho u_r dz, \tag{7}$$

whereas the mass ejected through the S_d surface can be found by:

$$\dot{M}_{ej} = \int_{S_d} \rho \mathbf{u} \cdot d\mathbf{S}. \tag{8}$$

The accretion rate takes into account both halves of the disk, under the equatorial symmetry assumption for density and radial velocity. Conversely the ejection rate of Eq. (8) includes only one of the jet beams (the counter-jet is not included).

In Fig. 4 we plot the ratio of the ejection to accretion flux including both jet and counter-jet, as a function of time for all four cases.

For magnetization values below equipartition the ejection efficiency $2\dot{M}_{ej}/\dot{M}_{acc}$ reaches a steady plateau. Stronger fields show no such behaviour. Table 1.1 summarizes some results on the accretion-ejection properties.

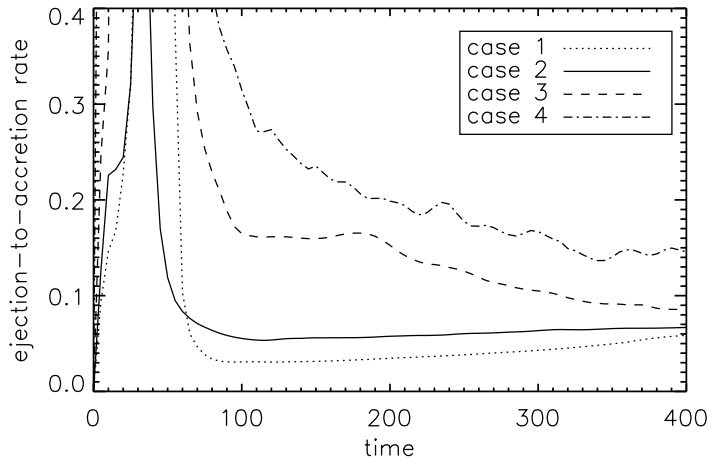

Figure 4: Mass ejection to accretion rates as a function of time, taking into consideration jet and counter jet: case 1 dotted, case 2 solid, case 3 dashed, case 4 dot-dashed. The trend shows an increase of the ratio as the magnetic field becomes stronger. Cases 3 and 4 decay into smaller values though as the ejection is not sustained. These two cases do not reach a steady configuration in contrast to the clear plateau reached for low magnetization configurations.

In terms of the ejection index ξ, defined as $\xi = d\ln\dot{M}_{acc}/d\ln r$, mass conservation in the control volume yields

$$\frac{2\dot{M}_{ej}}{\dot{M}_{acc}} = 1 - \left(\frac{r_i}{r_e}\right)^{\xi}. \tag{9}$$

From Eq. (9) it is clear that as the ejection efficiency increases so does the index. In accordance with analytical results (see Ferreira, 1997, Fig. 2), an increase in μ is accompanied by a gain in the ejection index ξ. Notice however that the analytical parameter space is quite narrow and does not encompass cases 1, 3 and 4 of our study. Also in agreement with the aforementioned study, due to the inefficiency of the magnetic acceleration, solutions with high ejection rates and large magnetizations do not allow super-Alfvénic outflows (Blandford & Payne, 1982, Wardle & Königl, 1993 and Ferreira, 1997).

In terms of the Keplerian velocity at the foot-point (at $R = 1.5R_{in}$), the terminal poloidal velocities reached for cases 1 to 4 are $\sim 4,3$, $\sim 4,5$, $\sim 1,8$ and $\sim 1,3$ respectively. This is in agreement also with the transformation rates of the magnetic field's energy to kinetic. The ratio of Poynting to kinetic flux is parametrized with $\sigma = -2\Omega r B_\phi B_p/\rho u^2 u_p$. Ω denotes the rotation rate of the magnetic surface. At the base of the outflow σ is proportional to the injection of energy into jets. We find that the available energy for the acceleration is

Table 1.1: Ejection Efficiency and Accretion Properties.

	plateau	$2\dot{M}_{ej}/\dot{M}_{acc}$	ξ	$\dot{M}_{acc;e}/\dot{M}_{acc;b}$	$V_{r;e}/V_{r;b}$
case1	yes	~ 0.06	0.027	2.12	6.1
case2	yes	~ 0.07	0.032	2.10	5.0
case3	no			1.31	4.5
case4	no			0.21	1.2

larger for low μ configurations, in agreement with the trend of the ejection index (as $\sigma \sim 1/\xi$ at the outflow's base). On top of that, the transformation rate for strongly magnetized cases is slower: since the magnetic surfaces are cylinders the conversion stops. From radial cuts in the upper end of the domain, the mean value of σ for cases 1 and 2 is of the order of $2-4\,10^{-1}$ whereas for cases 3 and 4 lies between $3-4$.

After the first qualitative estimate from the system's relaxation (Fig. 4), a more quantitative study of the MHD invariants along a field line can prove useful in the assessment of a steady state solution. MHD axisymmetric analytical models have certain quantities that must be conserved along any given magnetic surface in steady state configurations (Tsinganos, 1982): Ψ, the mass-to-magnetic flux ratio; Ω, the rotation rate of the magnetic surface; L, the specific angular momentum shared between the flow component and the magnetic field and E, the total energy-to-mass flux density. For cases below equipartition these quantities are all conserved along field lines anchored in the ejection region. Strong μ cases fail to meet this requirement.

The magnetic lever arm, defined at the Alfvénic surface as $\lambda = L/\Omega r_0^2 = (r_A/r_0)^2$, is also a value that must be conserved along the magnetic field line. Mediating the lever arm from different radii (1.5, 2.5, 3.5, 4.5 r_{in}) we find for case 1 $\lambda \sim 19.5$ and case 2 $\lambda \sim 17.5$, which are consistent with the formula $\lambda \sim 1 + 1/2\xi$ of Ferreira (1997). For cases of magnetization above equipartition this value is nonsensical due to their failure to properly cross the Alfvénic surface. As the magnetization increases we saw that the ejection index increases accordingly. The inverse happens for the specific angular momentum and lever arm, as ξ is analogous to the mass load, an increase of which results to lower L (confirming Blandford & Payne, 1982,Ouyed & Pudritz, 1997 and Ferreira, 1997).

In conclusion cases 1 and 2 reach a reasonably stationary state, while cases 3 and certainly 4, don't. This statement applies of course only to the innermost part of the magnetized disk, i.e the ejection region. The outer part, even for magnetization below equipartition, has not been allowed to evolve for an adequate number of revolutions to reach stationarity ($\sim 1/4$ rotations at $r = 40 r_{in}$).

At this point we wish to focus on some comparisons of global accretion-ejection simulations that include the accretion disk consistently with analytical solutions of adiabatically expanding outflows (Ferreira, 1997; Casse & Fer-

reira, 2000a). Simulations typically yield smaller magnetic lever arms and terminal velocities, as well as larger values of ejection indexes. Namely, for a configuration close to case 2 Ferreira (1997) would expect $\xi \sim 10^{-2}$, $\kappa \sim 2\,10^{-2}$ and $\lambda \sim 35$ with a terminal velocity of $V_{p\infty} = \Omega r_0 \sqrt{2\lambda - 3} \sim 8.2 V_K$, while in our case we found $\xi \sim 3\,10^{-2}$, $\kappa \sim 4\,10^{-2}$, $\lambda \sim 16$ and a terminal velocity only $\sim 4.5 V_K$. Even though such a configuration falls into the stable branch of the solutions found in Königl (2004), there is a deviation from the analytical expectations of Ferreira (1997). This could be attributed to some numerical effects, brought in by the returning current sheet which closes the current circuit inside the disk and the numerical dissipation on the disk surface. It should be stated though that our results are much closer to the analytical estimates if compared to previous studies (Casse & Keppens, 2002, 2004; Zanni et al., 2007).

4. Acknowledgments

This work was supported in part by the U.S. DoE under grant No. B523820 to the Center of Astrophysical Thermonuclear Flashes at the University of Chicago and the EU Marie Curie Research Training Network JETSET under contract MRTN-CT-2004-005592. Part of the simulations have been performed at CINECA, Bologna, Italy, under contract with INAF.

References

[1] R.D. Blandford 1976, MNRAS, 176, 465

[2] R.D. Blandford & D.G. Payne 1982, MNRAS, 199, 883

[3] F. Casse & J. Ferreira 2000a, A&A, 353, 1115

[4] F. Casse & J. Ferreira 2000b, A&A, 361, 1178

[5] F. Casse & R. Keppens 2002, ApJ, 581, 988

[6] F. Casse & R. Keppens 2004, ApJ, 601, 90

[7] J. Ferreira, J. & G. Pelletier 1995, A&A, 295, 807

[8] J. Ferreira 1997, A&A, 319, 340

[9] S.X. Kato, T. Kudoh, & K. Shibata 2002, ApJ, 565, 1035

[10] A. KÖNIGL 2004, ApJ, 617, 1267

[11] R.V.E. LOVELACE 1976, Nature, 262, 649

[12] A. MIGNONE, G. BODO, S. MASSAGLIA, T. MATSAKOS, O. TESILEANU, C. ZANNI, & A. FERRARI 2007, ApJS, 170, 228

[13] R. OUYED & R.E. PUDRITZ 1997, ApJ, 482, 712 and 484, 794

[14] N.I. SHAKURA & R.A. SUNYAEV 1973, A&A, 24, 337

[15] K. TSINGANOS 1982, ApJ, 252, 775

[16] Y. UCHIDA, & K. SHIBATA 1985, PASJ, 37, 515

[17] M. WARDLE, A. Königl 1993, ApJ, 410, 218

[18] C. ZANNI, A. FERRARI, R. ROSNER, G. BODO & S. MASSAGLIA 2007, A&A, 469, 811

Testo definitivo pervenuto in redazione il 20.5.2009.